HDL-TR-2171

November 1989

Symmetry, Selection Rules, and Energy Levels of $Pr^{3+}:Y_3Al_5O_{12}$

by John B. Gruber
Marian E. Hills
Roger M. Macfarlane
Clyde A. Morrison
Gregory A. Turner

U.S. Army Laboratory Command
Harry Diamond Laboratories
Adelphi, MD 20783-1197

The findings in this report are not to be construed as an official Department of the Army position unless so designated by other authorized documents.

Citation of manufacturer's or trade names does not constitute an official endorsement or approval of the use thereof.

Destroy this report when it is no longer needed. Do not return it to the originator.

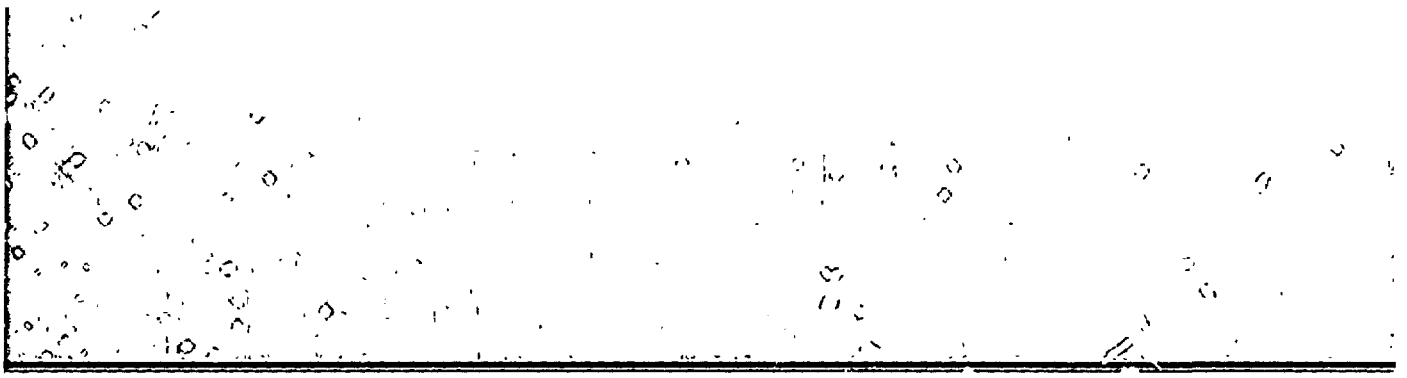

UNCLASSIFIED

SECURITY CLASSIFICATION OF THIS PAGE

ADA 215 120

REPORT DOCUMENTATION PAGE

Form Approved OMB No. 0704-0188

1a. REPORT SECURITY CLASSIFICATION Unclassified	1b. RESTRICTIVE MARKINGS
2a. SECURITY CLASSIFICATION AUTHORITY	3. DISTRIBUTION/AVAILABILITY OF REPORT Approved for public release; distribution unlimited.
2b. DECLASSIFICATION/DOWNGRADING SCHEDULE	
4. PERFORMING ORGANIZATION REPORT NUMBER(S) HDL-TR-2171	5. MONITORING ORGANIZATION REPORT NUMBER(S)
6a. NAME OF PERFORMING ORGANIZATION Harry Diamond Laboratories 6b. OFFICE SYMBOL (If applicable) SLCHD-ST-AP	7a. NAME OF MONITORING ORGANIZATION
6c. ADDRESS (City, State, and ZIP Code) 2800 Powder Mill Road Adelphi, MD 20783-1197	7b. ADDRESS (City, State, and ZIP Code)
8a. NAME OF FUNDING/SPONSORING ORGANIZATION Center for Night Vision and Electro-Optics 8b. OFFICE SYMBOL (If applicable)	9. PROCUREMENT INSTRUMENT IDENTIFICATION NUMBER
8c. ADDRESS (City, State, and ZIP Code) Ft. Belvoir, VA 22060	10. SOURCE OF FUNDING NUMBERS PROGRAM ELEMENT NO. 62120A; PROJECT NO. AH25; TASK NO.; WORK UNIT ACCESSION NO.

11. TITLE (Include Security Classification)

Symmetry, Selection Rules, and Energy Levels of $Pr^{3+}:Y_3Al_5O_{12}$

12. PERSONAL AUTHOR(S)

John B. Gruber, Marian E. Hills, Roger M. Macfarlane, Clyde A. Morrison, and Gregory A. Turner (see reverse)

13a. TYPE OF REPORT	13b. TIME COVERED	14. DATE OF REPORT (Year, Month, Day)	15. PAGE COUNT
Interim	FROM Aug 88 TO Oct 88	November 1989	34

16. SUPPLEMENTARY NOTATION

AMS code: 612120.H25; HDL Project: R8A951

17. COSATI CODES			18. SUBJECT TERMS (Continue on reverse if necessary and identify by block number)
FIELD	GROUP	SUB-GROUP	
20	02		Rare earth, crystal-field theory, $Pr^{3+}:Y_3Al_5O_{12}$, triply ionized praseodymium, YAG
20	05		

19. ABSTRACT (Continue on reverse if necessary and identify by block number)

Absorption, fluorescence, and site-selective excitation spectra of $Pr^{3+}:Y_3Al_5O_{12}$ are reported between 0.4 and 6.7 μm at several temperatures between 1.6 and 90 K. The complexity of the spectra indicates that Pr^{3+} ions occupy several different sites. The most intense spectra, representing the majority of the Pr^{3+} ions in dodecahedral lattice sites, are analyzed on the basis of electric-dipole selection rules for D_2 site symmetry. Weak spectra are reported but not analyzed because of the difficulty in assigning levels to a particular site. Analyses of intense spectra establish the symmetry of 17 Γ_1, 12 Γ_2, 10 Γ_3, and 12 Γ_4 Stark levels. These 51 levels are compared with the results of a crystal-field splitting calculation. A Hamiltonian consisting of Coulombic, spin-orbit, and crystal-field (D_2 symmetry) terms was diagonalized for all manifolds of the Pr^{3+} ($4f^2$) configuration. The rms deviation between calculated and experimental levels is 11 cm^{-1}.

20. DISTRIBUTION/AVAILABILITY OF ABSTRACT	21. ABSTRACT SECURITY CLASSIFICATION
☒ UNCLASSIFIED/UNLIMITED ☐ SAME AS RPT. ☐ DTIC USERS	Unclassified
22a. NAME OF RESPONSIBLE INDIVIDUAL Clyde A. Morrison	22b. TELEPHONE (Include Area Code) (202) 394-2042
	22c. OFFICE SYMBOL SLCHD-ST-AP

DD Form 1473, JUN 86 Previous editions are obsolete. SECURITY CLASSIFICATION OF THIS PAGE

UNCLASSIFIED

12 Cont'd. Personal Authors

J. Gruber, Department of Physics, San Jose State University, San Jose, CA 95192
M. Hills, Naval Weapons Center, Chemistry Division, China Lake, CA 93555
R. Macfarlane, IBM Almaden Research Center, San Jose, CA 95120
C. Morrison and G. Turner, Harry Diamond Laboratories

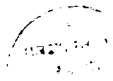

Contents

Figures

Tables

1. Introduction

The optical properties of trivalent rare-earth ions (R^{3+}) in yttrium aluminum garnet, $Y_3Al_5O_{12}$ (YAG), continue to be of great interest following recent developments in solid-state lasers and magneto-optical materials [1–5].* Over the years, the optical spectrum of Pr^{3+}:YAG has been studied by various groups [6–11], but there remain many uncertainties and ambiguities regarding the assignments. Although Pr^{3+} ions substitute predominantly for Y^{3+} ions in the dodecahedral sites of D_2 symmetry, several minority sites are occupied as well. This observation is not unique to Pr^{3+}:YAG, but is found for other R^{3+}:YAG materials as well [12–15]. Different sites can arise from defects caused by loss of oxygen from the lattice during crystal growth [16]. Consequently, increased attention has been placed on growing high-quality R^{3+}:YAG crystals.

We have investigated the spectroscopy of Pr^{3+}:YAG between 2,000 and 25,000 cm^{-1} at several temperatures between 1.6 and 90 K. In addition to absorption spectra, fluorescence from $^3P_0$ and site-selective emission spectra from $^1D_2$ were recorded. The most intense spectra, representing Pr^{3+} ions in D_2 sites, were analyzed according to electric-dipole selection rules for D_2 symmetry. The intense spectra included a number of hot bands that were analyzed. The analyses were aided by the knowledge that the ground state has Γ_3 symmetry and that the $^3P_0$ level has Γ_1 symmetry [8]. Fifty-one experimental Stark levels whose symmetry labels were established by this method of analysis were compared with a calculation that involved a Hamiltonian containing Coulombic, spin-orbit, and crystal-field terms in D_2 symmetry for all manifolds of the $4f^2$ configuration. The initial set of nine crystal-field parameters, B_{km}, was established from a lattice-sum calculation. By varying the crystal-field parameters, it was possible to obtain overall agreement between calculated and experimental levels with an rms deviation of 11 cm^{-1}. Additional levels, whose symmetry could not be established from experiment, were assigned from the results of the crystal-field calculation.

*References are listed at the end of the report.

2. Experimental Introduction

Two single crystals of Pr^{3+}:YAG were grown parallel to the <111> direction using the Czochralski method. The garnet melt was doped with praseodymium oxide, and the crystal growth took place in a nitrogen atmosphere containing 1000 ppm of oxygen. Discs were cut parallel to the (111) plane. The doping appeared to be uniform throughout the discs. Based on the distribution coefficient for the dopant, the crystals contained approximately 0.02 and 0.08 at. wt.% praseodymium based on yttrium. The concentrations as determined by electron-beam microprobe analysis were 0.018 and 0.072 at. wt.%, respectively.

A Nicolet model 7199 Fourier transform infrared (FTIR) spectrometer was used to obtain spectra between 1500 and 6000 cm^{-1}. The accuracy in determining the wavelength of the absorption peaks was limited by a combination of instrument resolution (0.25 cm^{-1}) and observed spectral linewidths. Absorption spectra between 2.5 and 0.4 μm (4,000 to 25,000 cm^{-1}) were measured with a Cary model 17D spectrophotometer. At 0.4 μm, the accuracy is better than 0.2 nm; the resolution is better than 0.1 nm. The precision in measuring the separation between peaks having apparent spectral linewidths of 0.2 nm is better than 0.02 nm. For data recorded at the same wavelength on both instruments, agreement is better than 2 cm^{-1}.

A conduction dewar filled with liquid nitrogen or liquid helium was used to obtain crystal spectra at nominally liquid nitrogen or liquid helium temperatures. At least 30 minutes was allowed for equilibration before spectra were obtained. Sample temperatures were not measured directly. However, from previous experience in taking similar spectra, we estimate the crystal temperatures as 90 and 15 K, respectively.

Absorption and emission spectra were also recorded between 0.4 and 0.8 μm using a 1.0-m Czerny-Turner Jarrell-Ash double monochromator with a resolution of 0.02 nm. The measured sample temperature in a liquid helium immersion cryostat was 1.6 K. Wavelengths were calibrated against the spectrum of neon. The wavelengths of the sharpest absorption peaks were determined with an accuracy of 0.05 nm.

3. Symmetry, Selection Rules, and Assignments

Yttrium aluminum garnet has cubic space group symmetry O_h^{10} ($Ia3d$) with eight formula units per unit cell [17,18]. The site symmetries of the ions are as follows: D_2 (Y^{3+}), C_{3i} (Al_1^{3+}), S_4 (Al_2^{3+}), and C_1 (O^{2-}). The Pr^{3+} ions that substitute for Y^{3+} ions on the dodecahedral sites experience a crystal field of D_2 symmetry. There are six magnetically inequivalent orientations of these sites in the crystal. The local x, y, and z axes of the Pr^{3+} ion sites are oriented along the (110), (1$\bar{1}$0), and (001) crystal axes (and the six equivalent directions) with a z-axis coinciding with the (001) crystal axis by convention [19].

The D_2 point group contains four one-dimensional irreducible representations, Γ_1, Γ_2, Γ_3, and Γ_4 according to Bethe notation [20]. For Pr^{3+} ($4f^2$), each $^{2S+1}L_J$ manifold is split into $2J + 1$ nondegenerate components (Stark levels). Table 1 gives the representations for each value of J up to 6. Table 2 presents the selection rules for electric-dipole transitions.

The dipole nature of the electronic transition is difficult to establish in crystals of R^{3+}:YAG because the overall symmetry is cubic. From linear dichroism measurements on samples with unequal site occupation, van der Ziel et al [8] observed only electric-dipole transitions in Pr^{3+}:YAG. They determined that the ground state has Γ_3 symmetry and the second excited Stark level at 50 cm^{-1} has either Γ_2 or Γ_4

Table 1. Full rotation compatibility table for D_2 group

J	Γ_1	Γ_2	Γ_3	Γ_4
0	1	0	0	0
1	0	1	1	1
2	2	1	1	1
3	1	2	2	2
4	3	2	2	2
5	2	3	3	3
6	4	3	3	3
Total[a]	28	21	21	21

[a] *Total number of Γ_n in electronic configuration $4f^2$.*

Table 2. Electric-dipole selection rules for D_2 symmetry

	Γ_1	Γ_2	Γ_3	Γ_4
Γ_1	—	y	z	x
Γ_2	y	—	x	z
Γ_3	z	x	—	y
Γ_4	x	z	y	—

symmetry. We chose Γ_4 symmetry for the level at 50 cm^{-1} on the basis of our crystal-field splitting calculation and the consistency we found in our analysis of hot-band data, which included transitions from the 50-cm^{-1} level.

For D_2 symmetry, electric-dipole transitions from the ground state to excited Stark levels having Γ_3 symmetry are forbidden. The absence of emission from the $^3P_0$ level, which has Γ_1 symmetry, to the first excited Stark level at 19 cm^{-1} indicates that the level has Γ_1 symmetry. Since electric-dipole transitions from the ground state to excited Stark levels having Γ_3 symmetry are forbidden, absorption lines corresponding to hot bands separated by 31 cm^{-1}, but lacking a low-temperature electronic origin, can be used to establish excited Γ_3 Stark levels.

Our analysis of the optical spectra reported in the next section is based on the following points:

a. Levels observed in the $^3P_0$ emission spectrum have either Γ_2, Γ_3, or Γ_4 symmetry; levels established from other measurements, but absent from the $^3P_0$ emission spectrum, have Γ_1 symmetry.

b. Levels observed in the $^1D_2$ emission have either Γ_1, Γ_3, or Γ_4 symmetry based on the analysis of the hot bands associated with the 16,409 cm^{-1} Stark level, which has Γ_2 symmetry; levels observed in emission spectra from both $^3P_0$ and $^1D_2$ have Γ_3 or Γ_4 symmetry; if the emission terminates on a level observed in absorption, then since the ground state has Γ_3 symmetry, the terminal level will have Γ_4 symmetry.

c. In absorption, if hot-band transitions are present that are 50 cm^{-1} to the low-energy side of a transition that persists at liquid helium temperature, but reveal no 19-cm^{-1} hot band, then the persisting transition is identified as one to an excited Γ_1 Stark level.

d. Levels observed in the absorption spectrum recorded at 1.6 K have Γ_1, Γ_2, or Γ_4 symmetry. If transitions to these levels show evidence of hot bands at 19 and 50 cm^{-1} to the low-energy side of the persisting transition, the excited states have Γ_2 symmetry.

e. Excited Γ_3 Stark levels can be located by observing a pair of hot bands in absorption separated by 31 cm^{-1} and inferring the energy of the forbidden $\Gamma_3 \rightarrow \Gamma_3$ transition.

f. If only a single 19-cm^{-1} hot band is associated with a transition that persists at liquid helium temperature, the excited Stark level has Γ_4 symmetry.

4. Absorption Spectra

Tables 3 to 5 (given at the end of this section) summarize the results of absorption measurements recorded at 1.6 K, liquid helium temperature (LHe), and liquid nitrogen temperature (LN). The observed spectra appear in figures 1 to 8. From the total number of absorption peaks observed, many of which are weak, it is clear that the Pr^{3+} ions occupy several kinds of sites. The weak peaks retain their relative strengths at low concentrations and hence are not thought to be associated with pairs or clusters of Pr^{3+} ions. It is difficult to determine whether weak peaks are due to weak transitions of Pr^{3+} ions in D_2 sites or strong transitions of Pr^{3+} ions in minority sites. Only the most intense spectra in a given manifold are assigned to transitions of Pr^{3+} ions in D_2 sites. These transitions are indicated in the fourth columns in tables 3 to 5.

Transitions corresponding to the strongest absorption peaks observed are identified using labels introduced by Dieke [21]. More than 100 temperature-dependent (hot-band) transitions were used to establish the first two excited Stark levels, Z_2 at 19 cm^{-1} and Z_3 at 50 cm^{-1}, in agreement with values reported earlier [7] and in agreement with the results obtained from the emission spectra from $^3P_0$ and $^1D_2$. The absence of a transition in absorption and emission between the 19 cm^{-1} ($^3H_4$) and 20,534 cm^{-1} ($^3P_0$) levels indicates that Z_2 (19 cm^{-1}) has Γ_1 symmetry. We chose Γ_4 symmetry for the 50-cm^{-1} level based on our crystal-field splitting calculation; the analysis of the hot-band data is consistent with this choice.

The infrared absorption spectra of the $^3H_5$, $^3H_6$, and $^3F_2$ manifolds recorded by the FTIR spectrometer are presented in figures 1 and 2. The absorption peaks become increasingly sharp toward the low-energy side of each manifold since the higher energy levels are broadened by spontaneous phonon emission. This is typical of solid-state rare-earth ion spectra. Multiphonon absorption due to the garnet lattice appears below 2200 cm^{-1}. The spectra recorded at LN temperature are reported in order to show several relatively intense transitions from Z_3 at 50 cm^{-1}. Similar, relatively intense hot bands originating from Z_3 are observed throughout the spectrum.

Figures 3 and 4 display the near-infrared absorption spectra of the $^3F_4$, $^3F_3$, and $^1G_4$ manifolds. Proximity between the $^3F_4$ and $^3F_3$ manifolds makes it necessary to consider a combined manifold of Stark levels for analysis. The intense sharp spectra and the hot-band assignments

generally agree with the analysis reported by Hooge [7]. The relatively weak $^1G_4$ absorption spectrum does not contain all the expected transitions. The lack of strong absorption peaks makes it difficult to determine the relative ordering among Stark levels and the overall splitting of the manifold. The predicted crystal-field splitting of the manifold suggests that not all the Stark levels have been observed.

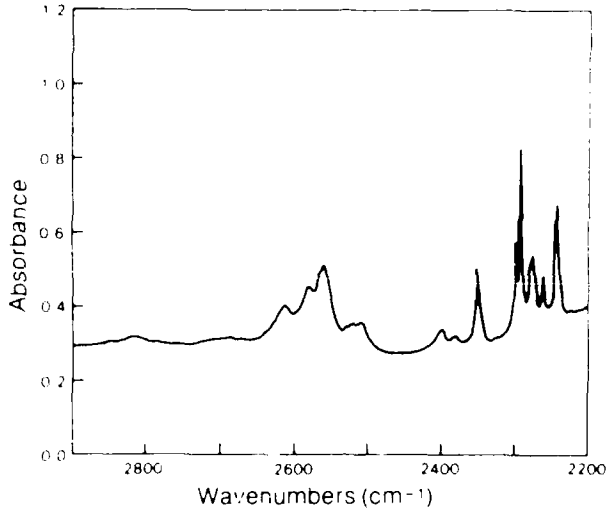

Figure 1. Absorption spectrum of $^3H_5$ manifold recorded at liquid nitrogen temperature.

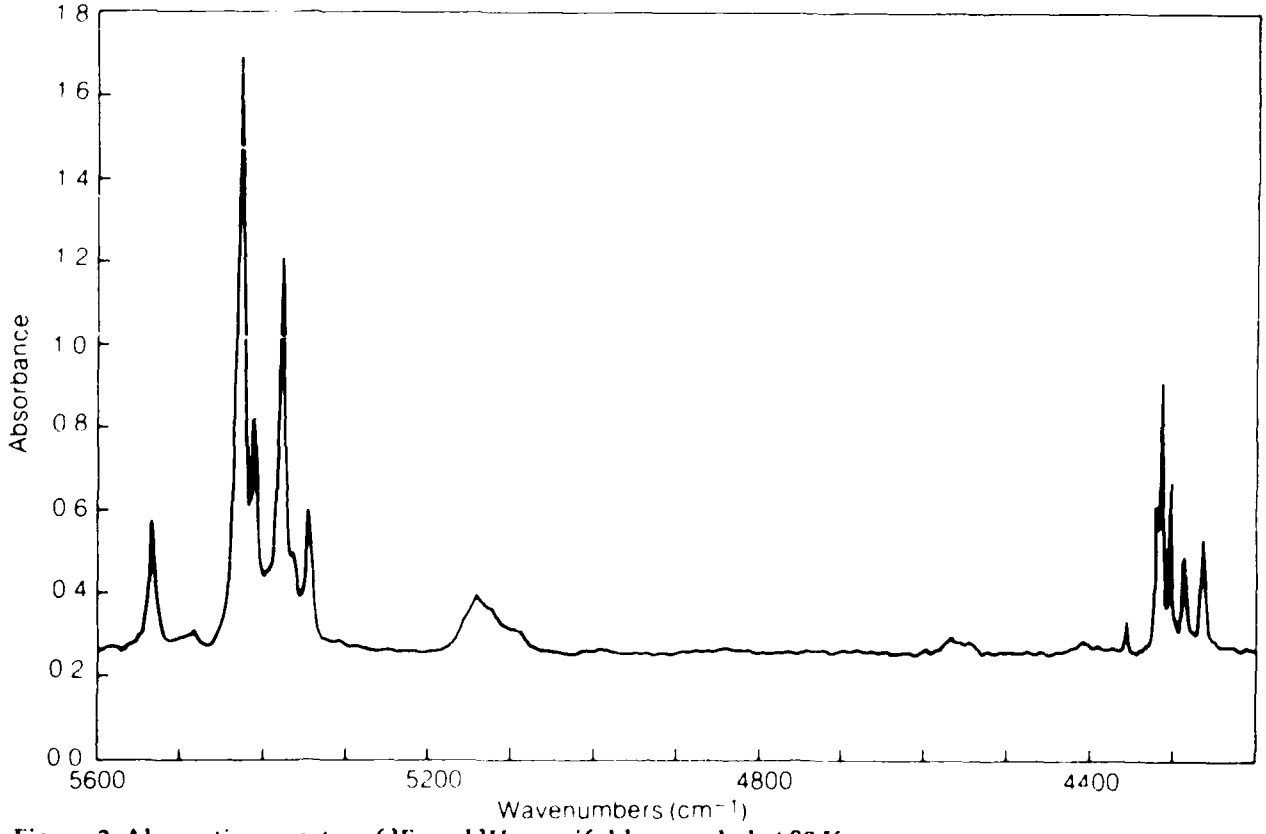

Figure 2. Absorption spectra of $^3F_2$ and $^3H_4$ manifolds recorded at 90 K.

To eliminate hot-band absorption entirely, absorption measurements of the $^1D_2$, $^3P_0$, $^3P_1$, $^1I_6$, and $^3P_2$ manifolds were made at 1.6 K. The result is the relatively simple spectra appearing in figures 5 to 8. Four principal absorption peaks, representing transitions from Z_1 to B_1, B_2, B_3, and B_5 of the $^1D_2$ manifold appear in figure 5 and are listed in table 5. From the higher temperature data, two hot bands 31 cm^{-1} apart establish the B_4 level at 17,088 cm^{-1}. The symmetry of the B_4 level is Γ_3, following the electric-dipole selection rules of table 2. Two weak peaks at 16,800 and 16,923 cm^{-1} are assigned to Pr^{3+} ions in other sites.

The $^3P_0$ absorption at 20,534 cm^{-1} ($Z_1 \rightarrow C_1$) (fig. 6) is assigned to Pr^{3+} ions in D_2 sites in agreement with earlier work [7–11]. The absorption is strong and is comparable to that observed from the ground state to levels W_3, V_2, V_5, B_2, E_1, and E_7. The weak peaks found on either side are attributed to Pr^{3+} ions in other sites. The intense peak at 20,534 cm^{-1} is also observed in fluorescence at 1.6 K. The predicted crystal-field splitting of the $^1I_6$ manifold (tables 6 and 7) is approximately 1500 cm^{-1}

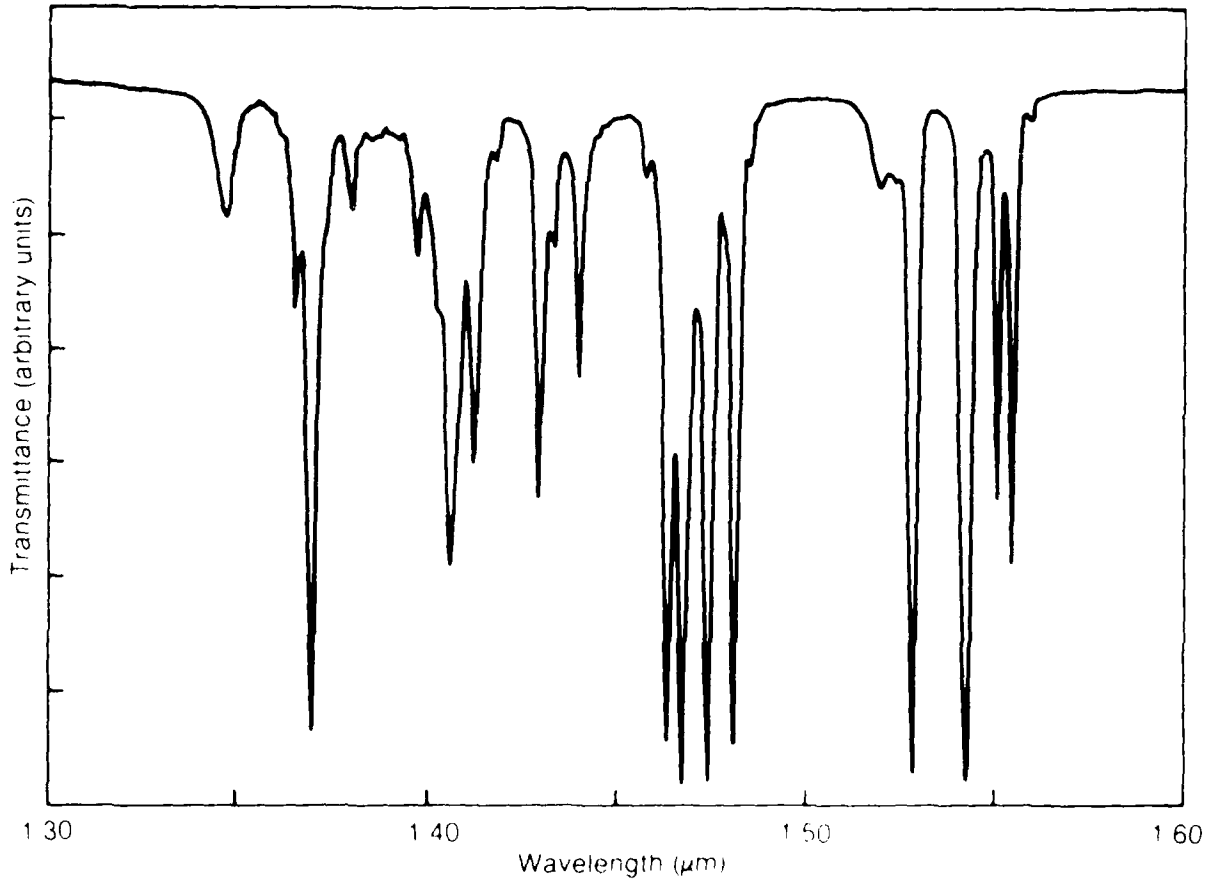

Figure 3. Absorption spectra of $^1F_4$ and $^1F_3$ manifolds recorded at 15 K.

and overlaps the predicted splitting of the $^3P_1$ manifold. We assume that the strong absorption at 1.6 K found at 21,045 and 21,113 cm^{-1} is part of the $^3P_1$ manifold since $^3H_4 \rightarrow {}^1I_6$ absorption is expected to be weak. Figure 7 indicates that only a few transitions to the $^1I_6$ manifold were observed. The number is insufficient to establish the overall splitting of the $^1I_6$ manifold. At 1.6 K, absorption peaks were observed at 20,805, 20,823, 21,667, and 21,869 cm^{-1}.

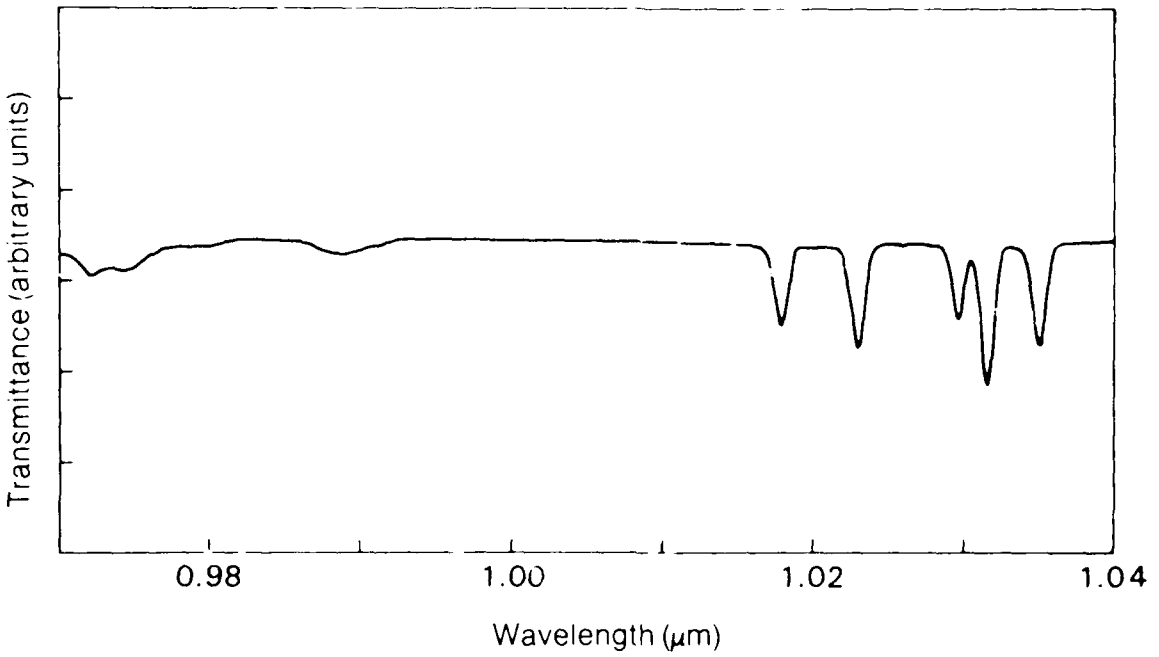

Figure 4. Absorption spectrum of $^1G_4$ manifold recorded at 15 K.

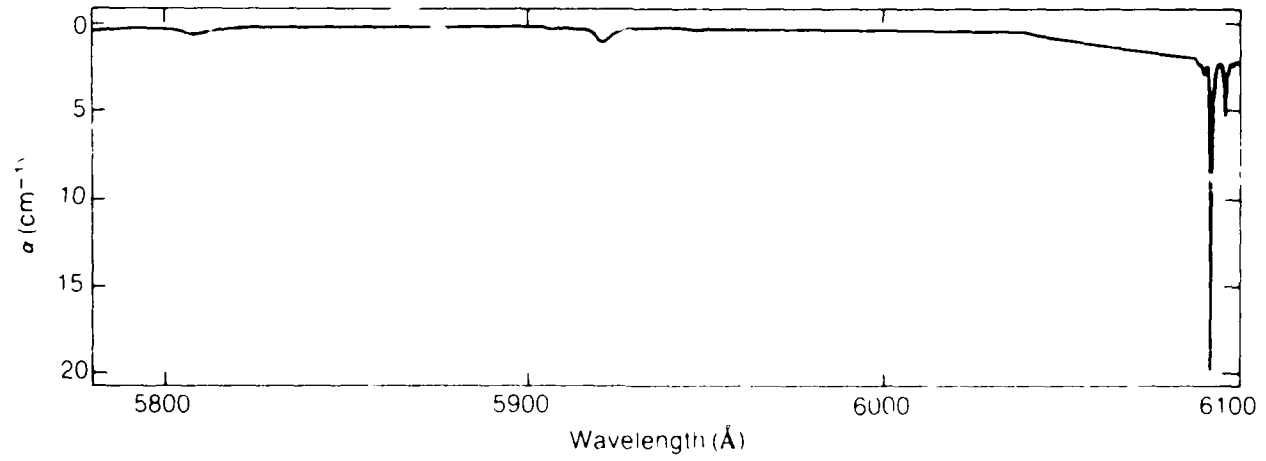

Figure 5. Absorption spectrum of $^1D_2$ manifold recorded at 1.6 K.

At 1.6 K the absorption to the $^3P_2$ manifold observed between 22,100 and 22,600 cm^{-1} consists of three peaks. Hot bands assist in making the following assignments: 22,103 (Γ_2), 22,153 (Γ_1), and 22,295 (Γ_1) cm^{-1}. Particularly noticeable even at 1.6 K (fig. 8) are the broad absorption bands that result from spontaneous phonon decay. A pair of hot bands places the Γ_3 level at 22,416 cm^{-1}.

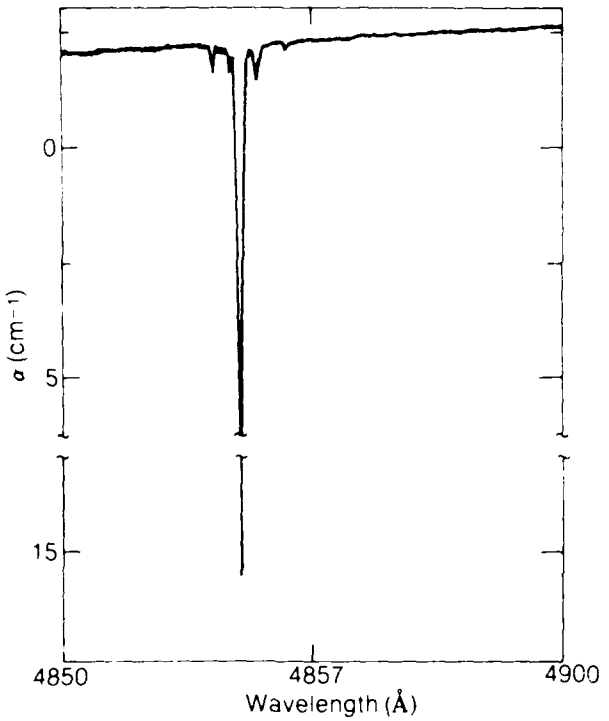

Figure 6. Absorption spectrum of $^3P_0$ at 1.6 K; four weak, sharp peaks clustered around intense peak suggest that Pr^{3+} ions are found in minority sites.

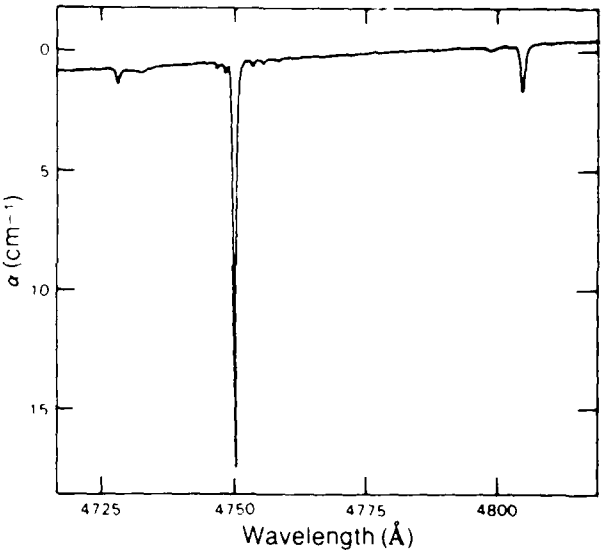

Figure 7. Absorption spectra of $^3P_1$ and $^1I_6$ manifolds recorded at 1.6 K.

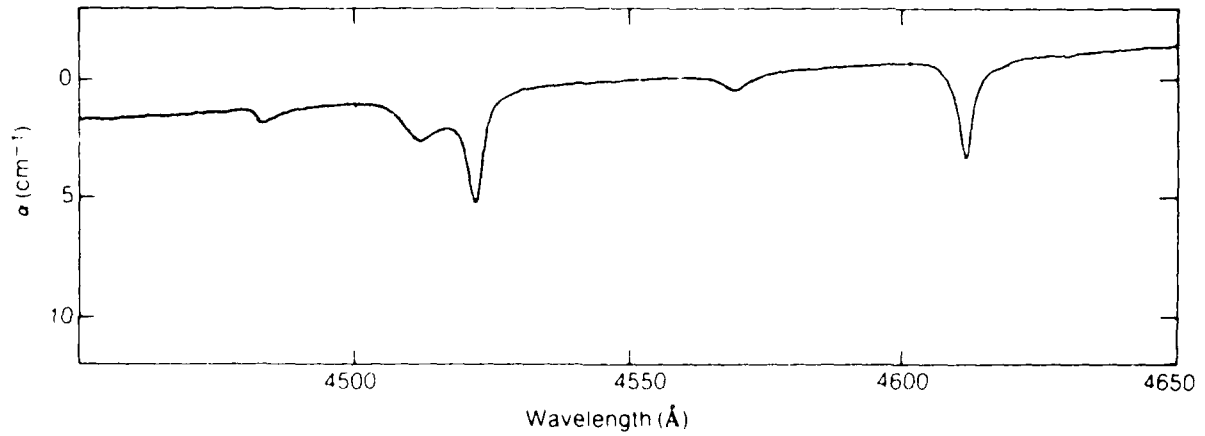

Figure 8. Absorption spectrum of $^3P_2$ manifold recorded at 1.6 K.

Table 3. Absorption and emission spectra of ^3H_J manifolds

Note: sh denotes shoulder; bd denotes broad; . . . indicates that presence of level is inferred (see sect. 3, paragraph e).

$^{2S+1}L_J$	E (cm^{-1})[a]	I[b]	Transition[c]	$^3P_0$[d] (cm^{-1})	$^1D_2$[e] (cm^{-1})	Level (cm^{-1})	Γ_a[g]
$^3H_4$	0	—	(Z_1)	0	0	0	3 (ref. 8)
	19	—	(Z_2)	—	18	19	1 (a, b, c)
	50	—	(Z_3)[h]	51	51	50	4 (a, b, f)
	—	—	(Z_m)	—	533	533	1 (a, b)
	—	—	(Z_n)	576	—	576	2–4 (a)
	—	—	(Z_o)	—	742	742	1 (a, b)
$^3H_5$	2209	<0.01	—	—	—	—	—
	2221	0.01	—	—	—	—	—
	2242*	0.27	$Z_3 \rightarrow Y_1$	—	—	—	—
	2261*	0.17	$Z_3 \rightarrow Y_3$	—	—	—	—
	2274*	0.20	$Z_2 \rightarrow Y_1$	—	—	—	—
	2280*	0.17	$Z_2 \rightarrow Y_2$	—	—	—	—
	2293	0.41	$Z_1 \rightarrow Y_1$	—	—	2293	2 (d)
	2299	0.36	$Z_1 \rightarrow Y_2$	2295	2295	2299	4 (a,b,f)
	. . .	. . .	(Y_3)	—	—	(2311)	3 (e)
	2347*(sh)	0.05	—	—	—	—	—
	2351	0.14	$Z_1 \rightarrow Y_4$	—	—	2351	1 (c)
	2380*	0.06	$Z_2 \rightarrow Y_5$	—	—	—	—
	2399	0.09	$Z_1 \rightarrow Y_5$	2398	2398	2399	(a,d)
	2520*	0.09	$Z_3 \rightarrow Y_6$	—	—	—	—
	2551*	0.10	$Z_2 \rightarrow Y_6$	—	—	—	—
	. . .	. . .	(Y_6)	—	—	(2570)	3 (e)
	2562*	0.20	$Z_2 \rightarrow Y_7$	—	—	—	—
	2581	0.18	$Z_1 \rightarrow Y_7$	2580	2580	2581	4 (a,b,f)
	2599	0.06	$Z_2 \rightarrow Y_9$	—	—	—	—
	2602	0.12	$Z_1 \rightarrow Y_8$	—	—	2602	1 (c)
	2618	0.10	$Z_1 \rightarrow Y_9$	—	—	2618	2 (d)
	2669	bd	—	—	—	—	—
	2688	bd	—	—	—	—	—
	2752	0.01	—	—	—	—	—
	2790*	0.02	$Z_3 \rightarrow Y_{11}$	—	—	—	—
	2800*	0.03	$Z_2 \rightarrow Y_{10}$	—	—	—	—
	2820	0.04	$Z_1 \rightarrow Y_{10}$	—	—	2820	4 (f)
	2822*(sh)	0.02	$Z_2 \rightarrow Y_{11}$	—	—	—	—
	. . .	. . .	(Y_{11})	2841	2841	2840	3 (a,b,c)
	2850	bd	—	—	—	—	—
$^3H_6$	4214	0.01	—	—	—	—	—
	4244	0.02	—	—	—	—	—
	4265*	0.11	$Z_3 \rightarrow X_2$	—	—	—	—
	4286*	0.11	$Z_2 \rightarrow X_1$	—	—	—	—
	4289*	0.12	$Z_3 \rightarrow X_3$	—	—	—	—
	4305	0.24	$Z_1 \rightarrow X_1$	—	—	4305	4 (f)
	4316	0.35	$Z_1 \rightarrow X_2$	—	—	4316	1 (c)

Table 3 (cont'd). Absorption and emission spectra of ^3H_J manifolds

$^{2S+1}L_J$	E (cm^{-1})[a]	I[b]	Transition[c]	$^3P_0$[d] (cm^{-1})	$^1D_2$[e] (cm^{-1})	Level[f] (cm^{-1})	Γ_i[g]
$^3H_6$	4321*	0.17	$Z_2 \rightarrow X_3$	—	—	—	—
(cont'd)	...	...	(X_3)	—	—	4339	3 (e)
	4347	0.01	—	—	—	—	—
	4358	0.06	$Z_1 \rightarrow X_4$	—	—	4358	1 (c)
	4391*	0.02	$Z_2 \rightarrow X_5$	—	—	—	—
	4403*(sh)	0.02	—	—	—	—	—
	4409	0.03	$Z_1 \rightarrow X_5$	—	—	4409	2 (d)
	4420*	0.02	$Z_2 \rightarrow X_6$	—	—	—	—
	...	...	(X_6)	—	—	4440	3 (e)
	4548*	0.03	$Z_2 \rightarrow X_7$	—	—	—	—
	4558*	0.02	—	—	—	—	—
	4567	0.04	$Z_1 \rightarrow X_7$	—	—	4567	4 (f)
	4793*	0.01	$Z_3 \rightarrow X_{11}$	—	—	—	—
	4824*	0.01	$Z_2 \rightarrow X_{11}$	—	—	—	—
	4843	0.02	$Z_1 \rightarrow X_{11}$	—	—	4843	2 (d)
	4994	0.02	$Z_3 \rightarrow X_{12}$	—	—	—	—
	5045	0.03	$Z_1 \rightarrow X_{12}$	—	—	5045	1 (c)
	5091	0.03	$Z_3 \rightarrow X_{13}$	—	—	—	—
	5122*	0.10	$Z_2 \rightarrow X_{13}$	—	—	—	—
	5141	0.12	$Z_1 \rightarrow X_{13}$	—	—	5141	2 (d)

[a] Absorption spectra recorded at LHe temperature for $^3H_6$, LN temperature for $^3H_5$; room temperature spectra for both manifolds were used to establish hot bands, denoted by *.

[b] Intensity in absorbance units.

[c] Transitions assigned to absorption spectra of Pr^{3+} in D_2 sites.

[d] Fluorescence spectrum from $^3P_0$ at 1.6 K.

[e] Selectively pumped fluorescence spectrum from $^1D_2$ at 1.6 K.

[f] Experimental energy levels assigned to Pr^{3+} in D_2 sites.

[g] D_2 symmetry representations Γ_1, Γ_2, Γ_3, and Γ_4; letters in parentheses refer to method of assignment described in sect. 3.

[h] Ref. 8 identifies Z_3 as either Γ_2 or Γ_4; observed emission from the 16,409 cm^{-1} level (which has Γ_2 symmetry based on an analysis of hot bands in the absorption spectrum) indicates that Z_3 has Γ_4 symmetry, in agreement with calculations in table 7.

Table 4. Absorption spectra of ^3F_J manifolds

Note: sh denotes shoulder; bd denotes broad; . . . indicates that presence of level is inferred (see sect. 3, paragraph e).

$^{2S+1}L_J$	E (cm^{-1})[a]	I[b]	Transition[c]	Level[d] (cm^{-1})	Γ_4^*
$^3F_2$	5290	<0.01	—	—	—
	5305	0.01	—	—	—
	5346*	0.32	$Z_2 \rightarrow W_1$	—	—
	5365	0.23	$Z_1 \rightarrow W_1$	5365	4 (f)
	5379*	0.92	$Z_3 \rightarrow W_2$	—	—
	5411*	0.55	$Z_2 \rightarrow W_2$	—	—
	5430	1.42	$Z_1 \rightarrow W_2$	5430	2 (d)
	5485*	0.05	$Z_3 \rightarrow W_4$	—	—
	5516*	0.04	$Z_2 \rightarrow W_4$	—	—
	. . .	. . .	(W_4)	(5535)	3 (c)
	5535*	0.32	$Z_3 \rightarrow W_5$	—	—
	5585	0.03	$Z_1 \rightarrow W_5$	5585	1 (c)
	5621	<0.01	—	—	—
$^3F_3$	6417*	0.20	$Z_3 \rightarrow V_1$	—	—
	6432*	0.70	$Z_3 \rightarrow V_2$	—	—
	6448*	0.86	$Z_2 \rightarrow V_1$	—	—
	. . .	. . .	(V_1)	(6467)	3 (c)
	6482	1.30	$Z_1 \rightarrow V_2$	6482	1 (c)
	6511	0.15	—	—	—
	6541*	1.30	$Z_2 \rightarrow V_3$	—	—
	6561	0.40	$Z_1 \rightarrow V_3$	6561	4 (f)
	6572	0.03	—	—	—
	6590	0.03	—	—	—
	6760	0.90	$Z_2 \rightarrow V_5$	—	—
	6779*(sh)	0.80	$Z_3 \rightarrow V_6$	—	—
	6781	1.40	$Z_1 \rightarrow V_5$	6781	4 (f)
	6812*	1.40	$Z_2 \rightarrow V_6$	—	—
	6831(sh)	1.12	$Z_1 \rightarrow V_6$	6831	2 (d)
	6857	0.02	—	—	—
	6876	0.02	—	—	—
	6943*	0.20	$Z_3 \rightarrow V_7$	—	—
	6973*	0.10	$Z_2 \rightarrow V_7$	—	—
	6994	0.30	$Z_1 \rightarrow V_7$	6994	2 (d)
$^3F_4$	7035*	0.06	$Z_3 \rightarrow U_3$	—	—
	7041*	0.05	$Z_2 \rightarrow U_2$	—	—
	7060	0.03	$Z_1 \rightarrow U_2$	7060	4 (f)
	7085	0.40	$Z_1 \rightarrow U_3$	7085	1 (c)
	7092*	0.30	$Z_3 \rightarrow U_4$	—	—
	7122*	0.65	$Z_2 \rightarrow U_4$	—	—
	7142	0.30	$Z_1 \rightarrow U_4$	7142	2 (d)
	7161	0.03	—	—	—
	7194*	0.05	$Z_3 \rightarrow U_5$	—	—

Table 4 (cont'd). Absorption spectra of ^3F_J manifolds

$^{2S+1}L_J$	E (cm^{-1})[a]	I[b]	Transition[c]	Level[d] (cm^{-1})	Γ_n^e
$^3F_4$ (cont'd)	7245	0.09	$Z_1 \rightarrow U_5$	7245	1 (c)
	7280*	0.06	$Z_2 \rightarrow U_6$	—	—
	7297	0.75	$Z_1 \rightarrow U_6$	7297	4 (f)
	7319	0.25	$Z_1 \rightarrow U_7$	7319	2 (d)
	7370*	0.05	$Z_3 \rightarrow U_8$	—	—
	7402*	0.10	$Z_2 \rightarrow U_8$	—	—
	...	...	(U_8)	(7421)	3 (e)
	7440*	0.10	$Z_3 \rightarrow U_9$	—	—
	7490	0.05	$Z_1 \rightarrow U_9$	7490	1 (c)

[a] Spectra recorded on spectrophotometer at LHe temperature.
[b] Intensity in absorbance units.
[c] Transitions assigned to spectra of Pr^{3+} in D_2 sites.
[d] Experimental energy levels assigned to Pr^{3+} in D_2 sites.
[e] D_2 symmetry representations given to assigned Stark levels; letters in parentheses refer to method of assignment described in sect. 3.

Table 5. Absorption spectra of $^1G_4$, $^1D_2$, $^3P_0$, $^1I_6$, $^3P_1$, and $^3P_2$ manifolds

Note: * refers to observed hot bands at LN temperature; sh denotes shoulder; bd = broad, usually very weak, Pr^{3+} site uncertain; . . . indicates that presence of level is inferred (see sect. 3, paragraph e).

$^{2S+1}L_J$	E (cm^{-1})[a]	I[b]	Transition[c]	E (cm^{-1})[d]	Level[e] (cm^{-1})	Γ_a[f]
$^1G_4$	9,667*	0.08	$Z_3 \rightarrow A_1$	—	—	—
	9,698*	0.12	$Z_2 \rightarrow A_1$	—	—	—
	9,717	0.06	$Z_1 \rightarrow A_1$	—	9,717	2 (d)
	9,775*	bd	—	—	—	—
	9,780*	0.10	$Z_3 \rightarrow A_4$	—	—	—
	9,828	0.07	$Z_1 \rightarrow A_4$	—	9,828	1 (c)
	10,096*	0.02	$Z_2 \rightarrow A_6$	—	—	—
	10,116	0.03	$Z_1 \rightarrow A_6$	—	10,116	4 (f)
	10,211*	0.01	$Z_3 \rightarrow A_7$	—	—	—
	10,262*	0.03	$Z_2 \rightarrow A_7$	—	—	—
	10,282	0.03	$Z_1 \rightarrow A_7$	—	10,282	2 (d)
	10,330*	0.02	$Z_3 \rightarrow A_8$	—	—	—
	10,360*	0.02	$Z_2 \rightarrow A_8$	—	—	—
	. . .	. . .	(A_8)	—	(10,380)	3 (e)
$^1D_2$	16,264	0.01	—	—	—	—
	16,324	0.02	—	—	—	—
	16,350*(sh)	0.30	$Z_3 \rightarrow B_1$	—	—	—
	16,358*	0.83	$Z_3 \rightarrow B_2$	—	—	—
	16,381(sh)	0.03	—	—	—	—
	16,390*	0.50	$Z_2 \rightarrow B_2$	—	—	—
	16,400	0.46	$Z_1 \rightarrow B_1$	16,400	16,400	1 (c)
	16,409	1.10	$Z_1 \rightarrow B_2$	16,410	16,409	2 (b,d)
	16,478	0.01	—	—	—	—
	16,755	0.01	—	—	—	—
	16,777	<0.01	—	—	—	—
	16,805	0.05	—	16,800	—	—
	16,830*	1.19	$Z_3 \rightarrow B_3$	—	—	—
	16,856	0.03	—	—	—	—
	16,881	0.33	$Z_1 \rightarrow B_3$	16,887	16,881	1 (c)
	16,903	0.03	—	—	—	—
	16,921	0.03	—	16,919	—	—
	16,956	<0.01	—	—	—	—
	17,037*	0.26	$Z_3 \rightarrow B_4$	—	—	—
	17,069*	0.06	$Z_2 \rightarrow B_4$	—	—	—
	. . .	. . .	($B4$)	—	(17,088)	3 (e)
	17,191(sh)*	0.07	$Z_2 \rightarrow B_5$	—	—	—
	17,210	0.17	$Z_1 \rightarrow B_5$	17,207	17,210	4 (f)
	17,250	bd	—	—	—	—
$^3P_0$	20,459	0.04	—	—	—	—
	20,483*	0.20	$Z_3 \rightarrow C_1$	—	—	—
	20,517	0.05	—	—	—	—
	20,534	0.60	$Z_1 \rightarrow C_1$	20,530	20,534	1 (a,c)

Table 5 (cont'd). Absorption spectra of $^1G_4$, $^1D_2$, $^3P_0$, $^1I_6$, $^3P_1$, and $^3P_2$ manifolds

$^{2S+1}L_J$	E (cm^{-1})[a]	I[b]	Transition[c]	E (cm^{-1})[d]	Level[e] (cm^{-1})	Γ_a[f]
$^1I_6$	20,681	0.02	—	—	—	—
and	20,701	0.03	—	—	—	—
$^3P_1$	20,755*	0.03	—	—	—	—
	20,781*	0.03	—	—	—	—
	20,786*	0.10	—	—	—	—
	20,805	0.20	—	20,805	—	—
	20,831	0.05	—	20,823	—	—
	20,942	<0.01	—	—	—	—
	20,950	<0.01	—	—	—	—
	20,994*	0.51	$Z_3 \rightarrow E_1$	—	—	—
	21,010*(sh)	0.04	—	—	—	—
	21,026*	0.23	$Z_2 \rightarrow E_1$	—	—	—
	21,045	1.32	$Z_1 \rightarrow E_1$	21,045	21,045	2 (d, $^3P_1$)
	21,087*	0.09	—	—	—	—
	21,093*	0.09	$Z_2 \rightarrow E_2$	—	—	—
	21,113	0.87	$Z_1 \rightarrow E_2$	21,113	21,113	4 (f, $^3P_1$)
	21,140	0.03[b]	—	21,135	—	—
	21,152*	0.25	—	—	—	—
	21,520*	0.03	—	—	—	—
	21,568*	0.05	—	—	—	—
	...	—	—	—	—	—
	21,588	0.15	—	—	—	—
	21,651*	0.60	—	—	—	—
	21,672	1.10	—	21,667	—	—
	21,732	0.03	—	—	—	—
	21,781	0.01	—	—	—	—
	21,810	0.01	—	—	—	—
	21,820*	0.10	—	—	—	—
	21,870	0.27	—	21,869	—	—
$^3P_2$	22,054*	0.50	$Z_3 \rightarrow F_1$	—	—	—
	22,084*	0.95	$Z_2 \rightarrow F_1$	—	—	—
	22,103	1.12	$Z_1 \rightarrow F_1$	22,100	22,103	2 (d)
	22,153	0.60	$Z_1 \rightarrow F_2$	22,150	22,153	1 (c)
	22,245*	0.14	$Z_3 \rightarrow F_3$	—	—	—
	22,295	0.25	$Z_1 \rightarrow F_3$	22,288	22,295	1 (c)
	22,367	0.08	$Z_1 \rightarrow F_4$	—	22,367	4 (f)
	22,397	0.12	$Z_2 \rightarrow F_5$	—	—	—
	...	...	(F_5)	—	(22,416)	3 (d)
	22,570	bd	—	—	—	—

[a] Spectra recorded on spectrophotometer at LHe temperature.

[b] Intensity in absorbance units.

[c] Transitions assigned to spectra of Pr^{3+} in D_2 sites.

[d] Spectra recorded at 1.6 K.

[e] Observed energy levels of Pr^{3+} in D_2 sites.

[f] D_2 symmetry representations given to assigned Stark levels; letters in parentheses refer to method of assignment given in sect. 3.

Table 6. Cubic O_h^{10} ($Ia3d$) 230

Lattice constant is 1.2 nm (ref. 18); crystallographic data on $Y_3Al_5O_{12}$

Ion	Site	Symmetry	x	y	z	q^a	α (Å^3)^b
Y	24c	D_2	0	1/4	1/8	3	0.870
Al_1	16a	C_{3i}	0	0	0	3	0.0530
Al_2	24d	S_4	0	1/4	3/8	q_{Al2}	0.0530
O	96h	C_1	x^c	y^c	z^c	q_O	1.349

[a] The values of q are in units of the electron charge with $4q_O + q_{Al2} = -5$.
[b] Ref. 26.
[c] $x = -0.0306$, $y = 0.0512$, $z = 0.150$ (ref. 18).

Table 7. Energy levels of Pr^{3+} ions in D_2 sites

Note: . . . indicates that presence of level is inferred (see sect. 3, paragraph e)

	Experimental[a]		Calculated[b]		
$^{2S+1}L_J$	E (cm^{-1})	Γ_n	E (cm^{-1})	Γ_n	Percent free-ion mixture[c]
$^3H_4$	0	3	−1	3	99.9 $^3H_4$ + 0.08 $^3H_5$ + 0.03 $^3F_3$
503	19	1	19	1	99.9 $^3H_4$ + 0.05 $^3F_2$ + 0.04 $^3H_5$
	50	4[e]	39	4	99.6 $^3H_4$ + 0.21 $^3H_5$ + 0.08 $^3F_2$
	. . .	. . .	495	2	95.2 $^3H_4$ + 3.55 $^3H_5$ + 1.03 $^3F_2$
	533	1[e]	505	1	98.1 $^3H_4$ + 0.77 $^3F_2$ + 0.43 $^3F_4$
	. . .	. . .	506	3	96.1 $^3H_4$ + 2.90 $^3H_5$ + 0.75 $^3F_3$
	576	4[e]	532	4	95.6 $^3H_4$ + 3.39 $^3H_5$ + 0.88 $^3F_3$
	742	1	755	1	93.6 $^3H_4$ + 5.17 $^3H_5$ + 0.91 $^3F_2$
	. . .	. . .	759	2	93.3 $^3H_4$ + 5.75 $^3H_5$ + 0.54 $^3F_3$
$^3H_5$	2293	2	2286	2	96.8 $^3H_5$ + 2.26 $^3H_4$ + 0.79 $^3F_2$
2595	2299	4	2270	4	95.5 $^3H_5$ + 3.28 $^3H_4$ + 0.42 $^3F_3$
	2311	3[e]	2291	3	97.3 $^3H_5$ + 1.34 $^3H_4$ + 1.09 $^3F_3$
	2351	1	2357	1	93.3 $^3H_5$ + 4.28 $^3H_4$ + 1.06 $^3F_2$
	2399	2	2412	2	95.1 $^3H_5$ + 3.59 $^3H_4$ + 0.45 $^3H_6$
	2570	3	2577	3	93.6 $^3H_5$ + 3.10 $^3F_2$ + 2.05 $^3H_6$
	2581	4	2583	4	94.4 $^3H_5$ + 2.73 $^3H_6$ + 1.06 $^3F_2$
	2602	1	2597	1	93.4 $^3H_5$ + 3.92 $^3F_2$ + 1.62 $^3H_6$
	2618	2[f]	2625	2	94.3 $^3H_5$ + 2.53 $^3H_6$ + 1.44 $^3H_4$
	2820	4	2824	4	92.4 $^3H_5$ + 4.71 $^3H_6$ + 2.25 $^3F_2$
	2840	3	2836	3	92.6 $^3H_5$ + 5.13 $^3H_6$ + 0.79 $^3F_2$
$^3H_6$	4305	4	4302	4	94.2 $^3H_6$ + 4.17 $^3F_2$ + 0.90 $^3H_5$
4744	4316	1	4325	1	95.9 $^3H_6$ + 2.97 $^3F_2$ + 0.49 $^3H_5$
	4339	3	4365	3	95.7 $^3H_6$ + 3.22 $^3F_2$ + 0.61 $^3F_4$
	4358	1	4347	1	95.3 $^3H_6$ + 3.37 $^3F_2$ + 0.60 $^3F_4$
	4409	2	4398	2	95.6 $^3H_6$ + 1.84 $^3H_5$ + 1.57 $^3F_4$
	4440	3	4431	3	93.6 $^3H_6$ + 3.89 $^3H_5$ + 0.96 $^3F_4$
	4567	4	4574	4	92.1 $^3H_6$ + 3.78 $^3H_5$ + 2.09 $^3F_4$
	. . .	. . .	4695	1	88.1 $^3H_6$ + 5.80 $^3F_4$ + 4.77 $^3F_2$
	. . .	. . .	4736	3	75.4 $^3H_6$ + 17.0 $^3F_2$ + 4.12 $^3F_3$
	. . .	. . .	4780	4	78.1 $^3H_6$ + 12.6 $^3F_2$ + 7.66 $^3F_3$
	4843	2	4843	2	86.8 $^3H_6$ + 7.99 $^3F_2$ + 2.53 $^3F_3$
	5045	1	5047	1	66.2 $^3H_6$ + 25.7 $^3F_2$ + 6.80 $^3F_3$
	5141	2[f]	5106	2	75.7 $^3H_6$ + 11.8 $^3F_2$ + 9.61 $^3F_3$

Table 7 (cont'd). Energy levels of Pr^{3+} ions in D_2 sites

$^{2S+1}L_J$	Experimental[a] E (cm^{-1})	Experimental[a] Γ_n	Calculated[b] E (cm^{-1})	Calculated[b] Γ_n	Percent free-ion mixture[c]
$^3F_2$	5365	4	5388	4	74.0 $^3F_2$ + 15.6 $^3H_6$ + 5.21 $^3F_4$
5292	...	...	5422	1	69.1 $^3F_2$ + 22.9 $^3H_6$ + 5.23 $^3F_4$
	5430	2	5424	2	83.4 $^3F_2$ + 14.6 $^3H_6$ + 1.14 $^3H_4$
	5535	3	5530	3	67.9 $^3F_2$ + 17.9 $^3H_6$ + 6.19 $^3F_4$
	5585	1	5575	1	83.1 $^3F_2$ + 11.0 $^3H_6$ + 2.64 $^3H_5$
$^3F_3$	6467	3	6470	3	78.3 $^3F_3$ + 14.3 $^3F_4$ + 5.61 $^3F_2$
6604	6482	1	6486	1	75.8 $^3F_3$ + 18.7 $^3F_4$ + 3.27 $^3F_2$
	6561	4	6577	1	71.0 $^3F_3$ + 22.4 $^3F_4$ + 3.35 $^3F_2$
	...	...	6761	3	95.7 $^3F_3$ + 1.25 $^3H_5$ + 1.18 $^3H_4$
	6781	4	6768	4	92.2 $^3F_3$ + 4.50 $^3F_4$ + 1.15 $^3H_4$
	6831	2[f]	6803	2	96.0 $^3F_3$ + 1.32 $^3H_5$ + 0.92 $^3H_4$
	6994	2	6999	2	54.6 $^3F_3$ + 32.4 $^3F_4$ + 12.3 $^3H_6$
$^3F_4$	...	...	7040	3	78.0 $^3F_4$ + 14.2 $^3F_3$ + 6.25 $^3H_6$
7111	7060	4[e]	7050	4	74.1 $^3F_4$ + 18.1 $^3F_3$ + 6.41 $^3H_6$
	7085	1	7088	1	73.1 $^3F_4$ + 16.6 $^3F_3$ + 8.10 $^3H_6$
	7142	2	7149	2	60.4 $^3F_4$ + 28.0 $^3F_3$ + 9.01 $^3H_6$
	7245	1	7250	1	93.5 $^3F_4$ + 4.24 $^3H_6$ + 1.07 $^1G_4$
	7297	4	7303	4	88.8 $^3F_4$ + 7.13 $^3F_3$ + 2.77 $^3H_6$
	7319	2	7314	2	97.3 $^3F_4$ + 1.20 $^3H_6$ + 0.87 $^3H_5$
	7421	3	7404	3	94.5 $^3F_4$ + 2.35 $^3H_6$ + 1.42 $^3F_3$
	7490	1	7488	1	95.3 $^3F_4$ + 1.90 $^1G_4$ + 1.69 $^3H_6$
$^1G_4$	...	...	9,693	3	98.2 $^1G_4$ + 0.76 $^3H_6$ + 0.62 $^3F_4$
10,042	...	...	9,716	1	98.2 $^1G_4$ + 0.63 $^3H_6$ + 0.57 $^3F_4$
	9,717	2[e]	9,721	2	97.7 $^1G_4$ + 1.47 $^3F_4$ + 0.58 $^3H_6$
	...	...	9,724	4	98.7 $^1G_4$ + 0.46 $^3H_6$ + 0.32 $^3F_4$
	9,828	1[e]	9,907	1	98.3 $^1G_4$ + 0.78 $^3H_6$ + 0.70 $^3F_4$
	10,116	4	10,118	4	99.0 $^1G_4$ + 0.32 $^1I_6$ + 0.25 $^3H_5$
	10,282	2	10,281	2	99.0 $^1G_4$ + 0.46 $^1I_6$ + 0.20 $^3H_5$
	10,380	3[e]	10,380	3	99.0 $^1G_4$ + 0.36 $^1I_6$ + 0.26 $^3H_5$
	...	...	10,916	1	96.8 $^1G_4$ + 1.82 $^3F_4$ + 1.19 $^1I_6$
$^1D_2$	16,400	1	16,411	1	99.7 $^1D_2$ + 0.12 $^3P_2$ + 0.08 $^1I_6$
16,883	16,409	2	16,417	2	99.5 $^1D_2$ + 0.17 $^3P_2$ + 0.14 $^1I_6$
	16,881	1	16,867	1	97.1 $^1D_2$ + 2.77 $^1I_6$ + 0.05 $^1G_4$
	17,088	3	17,082	3	97.6 $^1D_2$ + 2.31 $^1I_6$ + 0.05 $^1G_4$
	17,210	4[e]	17,117	4	97.4 $^1D_2$ + 2.28 $^1I_6$ + 0 12 $^1G_4$
$^3P_0$	20,534	1	20,534	1	83.0 $^3P_0$ + 15.9 $^1I_6$ + 0.73 $^3P_2$
$^1I_6$	...	...	20,555	1	84.1 $^1I_6$ + 15.6 $^3P_0$ + 0.14 $^3P_2$
	...	...	20,560	3	99.8 $^1I_6$ + 0.07 $^1G_4$ + 0.07 $^3P_2$
	...	...	20,681	4	99.9 $^1I_6$ + 0.08 $^3P_2$ + 0.02 $^1D_2$
	...	...	20,697	2	99.9 $^1I_6$ + 0.07 $^3P_2$ + 0.03 $^1D_2$
	...	...	20,937	2	99.9 $^1I_6$ + 0.04 $^3P_1$ + 0.02 $^3P_2$
	...	...	20,938	1	99.9 $^1I_6$ + 0.02 $^3P_2$ + 0.01 $^1G_4$

Table 7 (cont'd). Energy levels of Pr^{3+} ions in D_2 sites

$^{2S+1}L_J$	Experimental[a] E (cm^{-1})	Experimental[a] Γ_a	Calculated[b] E (cm^{-1})	Calculated[b] Γ_a	Percent free-ion mixture[c]
$^3P_1$	21,045	2	21,056	2	98.5 $^3P_1$ + 1.13 $^3P_2$ + 0.14 $^3F_3$
21,099	21,113	4	21,103	4	97.0 $^3P_1$ + 2.27 $^3P_2$ + 0.40 $^1I_6$
	...	...	21,237	3	99.3 $^3P_1$ + 0.31 $^3P_2$ + 0.09 $^1I_6$
$^1I_6$	...	...	21,456	1	87.7 $^1I_6$ + 9.93 $^3P_2$ + 2.11 $^1D_2$
21,250	...	...	21,527	3	96.0 $^1I_6$ + 2.82 $^3P_2$ + 0.95 $^1D_2$
	...	...	21,716	4	84.3 $^1I_6$ + 13.1 $^3P_2$ + 1.38 $^1D_2$
	...	...	21,834	3	88.9 $^1I_6$ + 9.79 $^3P_2$ + 0.92 $^1D_2$
	...	...	21,858	4	95.7 $^1I_6$ + 3.43 $^3P_2$ + 0.38 $^3P_1$
	...	...	21,876	2	95.5 $^1I_6$ + 3.82 $^3P_2$ + 0.42 $^1G_4$
	...	...	22,005	1	75.0 $^1I_6$ + 23.3 $^3P_2$ + 0.73 $^1G_4$
$^3P_2$	22,103	2	22,076	2	94.6 $^3P_2$ + 3.92 $^1I_6$ + 1.12 $^3P_1$
22,147	22,153	1	22,172	1	84.9 $^3P_2$ + 14.1 $^1I_6$ + 0.38 $^3P_0$
	22,295	1	22,317	1	80.4 $^3P_2$ + 18.8 $^1I_6$ + 0.48 $^1D_2$
	22,367	4	22,364	4	80.8 $^3P_2$ + 17.0 $^1I_6$ + 1.29 $^3P_1$
	22,416	3	22,410	3	86.8 $^3P_2$ + 12.4 $^1I_6$ + 0.43 $^1D_2$
$^1S_0$	...	...	46,950	1	99.8 $^1S_0$ + 0.08 $^1I_6$ + 0.06 $^1G_4$
46,900					

[a] Experimental energy levels and symmetry labels established from spectra reported in tables 3 to 5.

[b] Theoretical energy levels calculated using B_{km} (cm^{-1}): B_{20} (481), B_{22} (123), B_{40} (−146), B_{42} (−2248), B_{44} (−1139), B_{60} (−1653), B_{62} (−772), B_{64} (869), B_{66} (−656); rms deviation between 51 experimental and calculated levels is 11 cm^{-1}.

[c] Three largest terms of the percent free-ion mixture.

[d] Theoretical free-ion centroids of $^{2S+1}L_J$ manifolds using set of atomic parameters listed in section 6.

[e] Symmetry labels assigned with assistance from the calculation; data in tables 3 to 5 are compatible with these assignments.

[f] Original levels used in calculation in parentheses: 2618 (2613), 5141 (5121), 6831 (6812).

5. Fluorescence and Selective Excitation Spectra

Fluorescence and selective excitation experiments at 1.6 K further assist in the assignment of Stark levels. The results of emission from the $^1D_2$ and $^3P_0$ levels are given in table 3.

The 16,409 cm^{-1} Stark level of the $^1D_2$ manifold was excited directly using a single-frequency cw dye laser of 2-MHz bandwidth. The result was the elimination of a number of weak fluorescence peaks that are observed by nonselective excitation. This is important since the 16,381 cm^{-1} transition which terminates on the Z_2 (19 cm^{-1}) level has comparable intensity to peaks associated with Pr^{3+} ions in other sites. Notwithstanding the narrow excitation bandwidth, several weak peaks were still observed, showing that perturbed sites with small energy shifts are present.

Figure 9, the emission from $^1D_2$ to the $^3H_4$ manifold at 1.6 K, shows three sharp peaks and two bands, each of which contains a reasonably sharp peak. The three sharp peaks are assigned as transitions to the levels Z_1(0), Z_2(19), and Z_3(50), all in cm^{-1}. If the symmetry of each of these levels is Γ_3, Γ_1, and Γ_4, respectively, then the originating Stark level in $^1D_2$ has Γ_2 symmetry. This assignment within the $^1D_2$ manifold is consistent with analysis of the hot bands observed in absorption. The relatively sharp peak in each of the two bands is used to establish additional Stark levels at 533 cm^{-1} (Γ_1) and 742 cm^{-1} (Γ_1). The broader structure is assigned to phonon-assisted transitions.

The $^3P_0$ level was excited by the 476.5-nm Ar-ion laser line and subsequent nonradiative relaxation. Consequently, several sites were involved in the emission. However, by comparing the derived energy levels with those obtained from the $^1D_2$ emission and with energy levels reported earlier by Hooge [7], we could assign the emission spectrum to levels of Pr^{3+} ions in D_2 sites for the $^3H_4$ and $^3H_5$ manifolds (see table 3). Levels derived from the $^1D_2$ emission not observed in the $^3P_0$ emission were assigned to Γ_1 symmetry based on electric-dipole selection rules for D_2 symmetry.

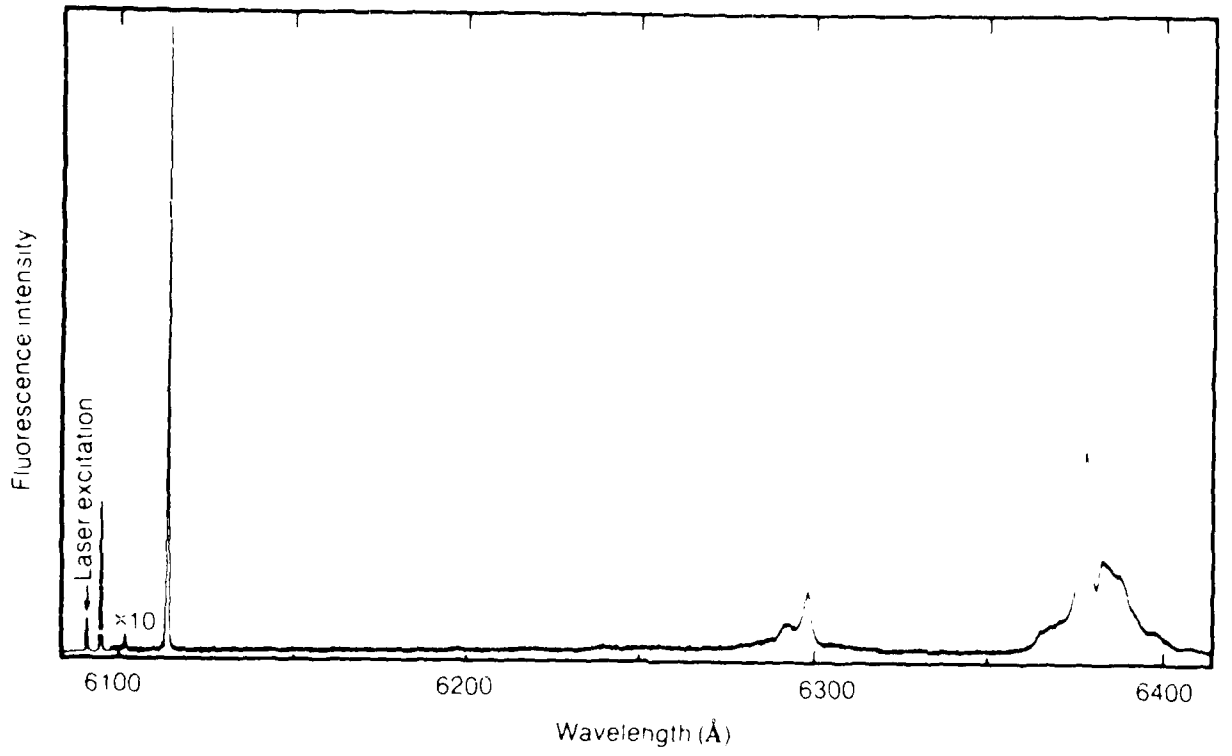

Figure 9. Site-selective laser excitation in $^1D_2$ manifold recorded at 1.6 K; emission is observed to $^3H_4$ ground state manifold.

6. Calculation of Crystal-Field Splitting

From the preceding analyses we have determined assignments for 17 Γ_1, 12 Γ_2, 10 Γ_3, and 12 Γ_4 experimental Stark levels. These 51 levels were compared with the results obtained from the following crystal-field splitting calculation.

The free-ion wave functions were determined by diagonalizing a Hamiltonian containing the Coulomb interaction described in terms of Racah parameters $E^{(1)}$, $E^{(2)}$, and $E^{(3)}$ and the spin-orbit interaction parameter ζ. Also included in the free-ion calculation was the inter-configuration interaction in terms of parameters α, β, and γ. All parameters were expressed in units of cm^{-1}. The values of the free-ion parameters used in our calculation were obtained from Carnall et al [22] and are

$E^{(1)} = 4548.2$,

$E^{(2)} = 21.935$,

$E^{(3)} = 466.73$,

$\zeta = 740.75$,

$\alpha = 21.255$,

$\beta = -799.94$, and

$\gamma = 1342.9$ (all in cm^{-1}).

The crystal-field splitting was calculated using the Hamiltonian [23]

$$H_{CF} = \sum_{ikm} B_{km} C_{km}(i) \ , \tag{1}$$

where

$$C_{km}(i) = \sqrt{\frac{4\pi}{2k+1}}\, Y_{km}(\theta_i, \phi_i) \tag{2}$$

and the sum over i covers the two electrons of the configuration $4f^2$ of Pr^{3+}. For D_2 symmetry there are nine nonvanishing B_{km} crystal-field parameters with even k. For the yttrium site in YAG there are six nonequivalent magnetic sites which are related by rotation operations. Explicit algebraic expressions for each set of B_{km} parameters associated with one of the six equivalent sets are given by Morrison and Leavitt [4]. We use the first set as defined by them (page 633, ref. 4).

The first determination of a set of B_{km} parameters was obtained from a lattice-sum calculation that included point-charge, point-dipole, and self-induced contributions [24,25]. Table 6 gives the ion positions in the lattice, effective ionic electric charges, and the polarizability of the oxygen ions [26]. The parameters A_{km} (table 7) are related to the B_{km} parameters through the expression

$$B_{km} = \rho_k(Pr)\ A_{km}\ , \qquad (3)$$

where $\rho_k(Pr)$ are radial factors [25]. The lattice-sum results provided an initial view of the overall splitting before the B_{km} parameters were varied to improve agreement with experimental energy levels and symmetry assignments.

Next, an empirical set of B_{km} parameters was determined from the best quadratic fit of B_{km} parameters obtained from earlier analyses of the observed spectra of Nd^{3+}, Tb^{3+}, Dy^{3+}, and Er^{3+} in YAG [24]. The calculated splitting using these parameters was in reasonable agreement with the splitting observed in Pr^{3+}:YAG. Subsequent variation of the parameters affected the symmetry assignment for only a few Stark levels. From these calculations, Z_3 (50 cm^{-1}) was assigned Γ_4 symmetry. This choice proved to be consistent in analyzing the 50-cm^{-1} hot bands and was the only exception to our algorithm of assigning symmetry labels to observed Stark levels.

Using established Γ_1 and Γ_3 experimental levels in the calculation, we allowed the B_{km} parameters to vary to obtain the best overall agreement between calculated and experimental levels. With the new set of parameters, we then predicted the splitting of the Γ_2 and Γ_4 levels and compared these results with our experimental levels. This calculation again predicted Z_3 (50 cm^{-1}) to have Γ_4 symmetry. A subsequent calculation including all 51 levels with their experimentally established symmetry labels was performed, giving a best overall rms deviation of 11 cm^{-1}. An additional six Stark levels, whose symmetry could not be established from experiment without some ambiguity, were identified through the results of the calculation. Table 7 compares the calculated and experimental levels for all manifolds.

7. Comments

With few exceptions, predicted splittings and symmetry assignments for the $^3H_4$, $^3H_5$, and $^1D_2$ manifolds are in agreement with levels and assignments established from emission and hot-band absorption data. Fluorescence from the $^3P_0$ manifold to a 576-cm^{-1} Stark level indicates that the level has Γ_2, Γ_3, or Γ_4 symmetry. Small changes in B_{km} parameters greatly affect the predicted splitting of $^3H_4$. The ground-state and excited Stark levels at 19 cm^{-1} and 50 cm^{-1} are observed in both emission and absorption. The Γ_n labels deduced from the emission spectra agree with those deduced from the absorption spectra. Our results differ in some details from other results reported recently [9,11], in which higher concentrations of Pr^{3+} or higher temperatures were used.

Level Y_5 in the $^3H_5$ manifold is predicted to have Γ_2 symmetry. This is in agreement with an analysis of the hot bands observed in the absorption spectrum. However, the fluorescence spectra suggest a Γ_4 symmetry. Since $^3H_5$ has only three Γ_4 levels, we chose the three levels for which emission, absorption, and the crystal-field splitting calculation were all in agreement (namely Y_2, Y_8, and Y_{10}) as Γ_4 levels. We assigned Y_5 to Γ_2 symmetry in agreement with absorption data and the prediction by the crystal-field splitting calculation.

Emission from $^3P_0$ and $^1D_2$ to the $^3H_6$ manifold is generally very weak [7,9]. Hooge [7] reports fluorescence from $^3P_0$ to Stark levels at 4296, 4333, 4396, 4451, and 4561 cm^{-1}. These levels correspond to levels established from our absorption data as follows: 4305 (Γ_4), 4339 (Γ_3), 4409 (Γ_2), 4440 (Γ_3), and 4567 (Γ_4) cm^{-1}. The selection rules are consistent in analyzing both the emission and absorption data for $^3H_6$. The crystal-field splitting calculation (table 7) is also in agreement with these assignments, although the 4339 (Γ_3) cm^{-1} level is predicted to lie somewhat higher. Levels not observed in emission from $^3P_0$ but identified from hot-band absorption data include 4316 (Γ_1), 4358 (Γ_1), 5045 (Γ_1), and 5141 (Γ_2) cm^{-1}. These levels agree with the calculated splitting given in table 7.

A small change in calculated splitting of the six highest energy Stark levels of the $^3H_6$ manifold has a great influence on the calculated splitting of the $^3F_2$ manifold. Unfortunately, we have experimental data on only three of these levels: 4843 (Γ_2), 5045 (Γ_1), and 5141 (Γ_2) cm^{-1}. Consequently, we reexamined our hot-band data and the reported levels for the $^3F_2$ manifold [7,9]. There are several intense hot

bands at 5379 and at 5535 cm^{-1} that persist even in the 15 K absorption spectrum. Furthermore, a pair of hot bands separated by 31 cm^{-1} implies a Γ_3 level at 5535 cm^{-1}, a level reported by others [7,9]. We chose W_1 (5365 cm^{-1}) to have Γ_4 symmetry since we found no evidence for a 50-cm^{-1} hot band. The calculation predicts a Γ_4 level at 5388 cm^{-1}. Hot-band data indicate that W_2 (5430 cm^{-1}) has Γ_2 symmetry and that W_5 (5585 cm^{-1}) has Γ_1 symmetry, in agreement with the calculated splitting.

The experimental assignments given to Stark levels of the $^3F_3$ and $^3F_4$ manifolds are in agreement with the calculated splitting. With only a few minor exceptions, our levels agree with those reported by Hooge [7]. The predicted splitting of the $^1G_4$ manifold was the most difficult to reconcile with experiment, since we could identify only some of the Stark levels out of the nine expected in D_2 symmetry. The predicted manifold splitting is over 1200 cm^{-1} (see table 7), with the four lowest energy levels found within 33 cm^{-1} of each other. A pair of hot bands separated by 31 cm^{-1} places a Γ_3 level at 10,380 cm^{-1}. The level observed at 9828 cm^{-1} appears to have Γ_1 symmetry, in agreement with Hooge [7]. The predicted level is nearly 80 cm^{-1} away from the observed level. We could not reduce this difference without affecting the overall agreement obtained for other established experimental levels used in the calculation.

The predicted splitting of the $^1D_2$ manifold is over 700 cm^{-1}. All five expected Stark levels and their symmetries have been identified from experiment; the calculated splitting is in reasonable agreement. Throughout all variations of B_{km} parameters, the two lowest Stark levels, having symmetry labels Γ_1 and Γ_2, would interchange positions as the lowest energy level in the manifold. Site-selective excitation from the 16,409 cm^{-1} level is consistent with the assignment of Γ_2 symmetry, which is based on an analysis of the hot-band data in absorption.

Table 7 indicates that the predicted splitting of the $^1I_6$ manifold overlaps the $^3P_1$ manifold. Our assignments to the $^3P_0$ and $^3P_1$ manifolds agree with work reported earlier [7,9]. The limited number of observed spectra associated with the $^1I_6$ precluded an analysis of the splitting of this manifold. Assignments given to the Stark levels of the $^3P_2$ manifold are in agreement with results from the crystal-field splitting calculation.

8. Conclusions

From an analysis of the emission and absorption spectra of Pr^{3+}:YAG, a number of Stark levels have been assigned to Pr^{3+} ions occupying Y^{3+} ion sites of D_2 symmetry in the garnet lattice. The most intense spectra can be analyzed with consistency. However, the origin of the weak spectra is uncertain, since some Pr^{3+} ions are found in minority sites. On the basis of 51 Stark levels assigned to Pr^{3+} ions in D_2 sites, comparison between experimental and calculated levels using the B_{km} parameters given in table 7 yields an rms deviation of 11 cm^{-1}.

Acknowledgments

The authors wish to thank M. Kokta, Union Carbide Corporation, Washougal, WA, for providing the samples and M. Nadler, Chemistry Division, Naval Weapons Center, China Lake, CA, for recording the FTIR spectra. JBG wishes to thank the American Society for Engineering Education for their support while spectra were taken at the Naval Weapons Center.

References

[1] L. G. DeShazer, ed., Proc. SPIE **681** (1986), 1160.

[2] V. V. Pologrudov, E. N. Karnaukhov, E. F. Martynovich, S. A. Smirnova, and A. G. Davydchenko, Opt. Spectrosc. (USSR) **59** (1985), 677.

[3] C. M. Wong, S. R. Rotman, and C. Warde, Appl. Phys. Lett. **44** (1984), 1038.

[4] C. A. Morrison and R. P. Leavitt, *Spectroscopic Properties of Triply Ionized Lanthanides in Transparent Host Crystals*, in *Handbook on the Physics and Chemistry of Rare Earths*, vol. 5, eds. K. A. Gschneidner, Jr., and L. E. Eyring, North-Holland, Amsterdam (1982).

[5] A. A. Kaminskii, *Laser Crystals*, Springer, New York (1981).

[6] E. Y. Wong, O. M. Stafsudd, and D. R. Johnston, J. Chem. Phys. **39** (1963), 780.

[7] F. N. Hooge, J. Chem. Phys. **45** (1966), 4504.

[8] J. P. van der Ziel, M. D. Sturge, and L. G. Van Uitert, Phys. Rev. Lett. **27** (1971), 508.

[9] E. Antic-Fidancev, M. Lemaître-Blaise, and P. Caro, Inorg. Chimica Acta **139** (1987), 281.

[10] O. L. Malta, E. Antic-Fidancev, M. Lemaître-Blaise, J. Dexpert-Ghys, and B. Piriow, Chem. Phys. Lett. **129** (1986), 557.

[11] V. V. Ryabchenkov, Sov. Phys. Crystallogr. **32** (1987), 855.

[12] M. Asano and J. A. Koningstein, Chem. Phys. **42** (1979), 369.

[13] E. V. Antonov, Kh. S. Bagdasarov, N. A. Kazakov, N. A. Kulagin, and L. P. Podus, Sov. Phys. Crystallogr. **29** (1984), 106.

[14] Yu. K. Voronko and A. A. Sobol, Phys. Status Solidi **27** (1975), 257.

[15] R. Bayerer, J. Heber, and D. Mateika, Z. Phys. B **64** (1986), 201.

[16] M. Kokta, Union Carbide Corporation, Washougal, WA (1987), private communication.

[17] S. Geller, Z. Kristollogr. **125** (1967), 1.

[18] F. Euler and J. A. Bruce, Acta Crystallogr. **19** (1965), 971.

[19] J. F. Dillon and L. R. Walker, Phys. Rev. **124** (1961), 1401.

[20] H. Bethe, Ann. Physik **3** (1929), 133.

[21] G. M. Dieke, *Spectra and Energy Levels of Rare Earth Ions in Crystals*, eds. H. M. Crosswhite and H. Crosswhite, Interscience, New York (1968).

[22] W. T. Carnall, P. R. Fields, and K. Rajnak, J. Chem. Phys. **49** (1968), 4424.

[23] B. R. Judd, *Operator Techniques in Atomic Spectroscopy*, McGraw-Hill, New York (1963).

[24] C. A. Morrison, D. E. Wortman, and N. Karayianis, J. Phys. C **9** (1976), L191.

[25] D. E. Wortman, C. A. Morrison, and N. Karayianis, *Rare Earth Ion-Host Lattice Interactions, 11.—Lanthanides in* $Y_3Al_5O_{12}$, Harry Diamond Laboratories, HDL-TR-1773 (1976).

[26] P. A. Schmidt, A. Weiss, and T. P. Das, Phys. Rev. B **19** (1979), 5525.

DISTRIBUTION

ADMINISTRATOR
DEFENSE TECHNICAL INFORMATION CENTER
ATTN DTIC-DDA (12 COPIES)
CAMERON STATION, BUILDING 5
ALEXANDRIA, VA 22314-6145

DIRECTOR
NIGHT VISION & ELECTRO-OPTICS CENTER
ATTN TECHNICAL LIBRARY
ATTN R. BUSER
ATTN A. PINTO
ATTN J. HABERSAT
ATTN R. RHODE
ATTN W. TRESSEL
FT BELVOIR, VA 22060

DIRECTOR
DEFENSE NUCLEAR AGENCY
ATTN TECH LIBRARY
WASHINGTON, DC 20305

UNDER SECRETARY OF DEFENSE RES
& ENGINEERING
ATTN TECHNICAL LIBRARY, 3C128
WASHINGTON DC 20301

OFFICE OF THE DEPUTY CHIEF OF STAFF,
FOR RESEARCH, DEVELOPMENT, &
ACQUISITION
DEPARTMENT OF THE ARMY
ATTN DAMA-ARZ-B, I. R. HERSHNER
WASHINGTON, DC 20310

COMMANDER
US ARMY ARMAMENT MUNITIONS &
CHEMICAL COMMAND (AMCCOM)
US ARMY ARMAMENT RESEARCH &
DEVELOPMENT CENTER
ATTN DRDAR-TSS, STINFO DIV
DOVER, NJ 07801

COMMANDER
ATMOSPHERIC SCIENCES LABORATORY
ATTN TECHNICAL LIBRARY
WHITE SANDS MISSILE RANGE, NM 88002

DIRECTOR
US ARMY BALLISTIC RESEARCH LABORATORY
ATTN SLCBR-DD-T (STINFO)
ABERDEEN PROVING GROUND, MD 21005

DIRECTOR
US ARMY ELECTRONICS WARFARE
LABORATORY
ATTN J. CHARLTON
ATTN DELET-DD
FT MONMOUTH, NJ 07703

COMMANDING OFFICER
USA FOREIGN SCIENCE & TECHNOLOGY CENTER
FEDERAL OFFICE BUILDING
ATTN DRXST-BS, BASIC SCIENCE DIV
CHARLOTTESVILLE, VA 22901

COMMANDER
US ARMY MATERIALS & MECHANICS
RESEARCH CENTER
ATTN DRXMR-TL, TECH LIBRARY
WATERTOWN, MA 02172

US ARMY MATERIEL COMMAND
5001 EISENHOWER AVE
ALEXANDRIA, VA 22333-0001

US ARMY MATERIEL SYSTEMS ANALYSIS
ACTIVITY
ATTN DRXSY-MP (LIBRARY)
ABERDEEN PROVING GROUND, MD 21005

COMMANDER
US ARMY MISSILE & MUNITIONS
CENTER & SCHOOL
ATTN ATSK-CTD-F
ATTN DRDMI-TB, REDSTONE SCI INFO CENTER
REDSTONE ARSENAL, AL 35809

COMMANDER
US ARMY RESEARCH OFFICE (DURHAM)
ATTN J. MINK
ATTN M. STROSIO
ATTN M. CIFTAN
ATTN B. D. GUENTHER
PO BOX 12211
RESEARCH TRIANGLE PARK, NC 27709

COMMANDER
US ARMY RSCH & STD GRP (EUROPE)
FPO NEW YORK 09510

COMMANDER
US ARMY TEST & EVALUATION COMMAND
ATTN D. H. SLINEY
ATTN TECH LIBRARY
ABERDEEN PROVING GROUND, MD 21005

COMMANDER
US ARMY TROOP SUPPORT COMMAND
ATTN DRXRES-RTL, TECH LIBRARY
NATICK, MA 01762

OFFICE OF NAVAL RESEARCH
ATTN J. MURDAY
ARLINGTON, VA 22217

DISTRIBUTION (cont'd)

DIRECTOR
NAVAL RESEARCH LABORATORY
ATTN CODE 2620, TECH LIBRARY BR
ATTN G. QUARLES
ATTN G. KINTZ
ATTN A. ROSENBAUM
ATTN G. RISENBLATT
ATTN CODE 5554, F. BARTOLI
ATTN CODE 5554, L. ESTEROWITZ
ATTN CODE 5554, R. E. ALLEN
WASHINGTON, DC 20375

COMMANDER
NAVAL WEAPONS CENTER
ATTN CODE 3854, R. SCHWARTZ
ATTN CODE 3854, M. HILLS (10 COPIES)
ATTN CODE 3844, M. NADLER
ATTN CODE 385, R. L. ATKINS
ATTN CODE 343, TECHNICAL INFORMATION DEPARTMENT
CHINA LAKE, CA 93555

AIR FORCE OFFICE OF SCIENTIFIC RESEARCH
ATTN MAJOR H. V. WINSOR, USAF
BOLLING AFB
WASHINGTON, DC 20332

HQ, USAF/SAMI
WASHINGTON, DC 20330

DEPARTMENT OF COMMERCE
NATIONAL BUREAU OF STANDARDS
ATTN LIBRARY
WASHINGTON, DC 20234

NASA LANGLEY RESEARCH CENTER
ATTN N. P. BARNES (2 COPIES)
ATTN G. ARMAGAN
ATTN P. CROSS
ATTN D. GETTENY
ATTN J. BARNES
ATTN E. FILER
ATTN C. BAIR
ATTN N. BOUNCRISHANI
HAMPTON, VA 23665

DIRECTOR
ADVISORY GROUP ON ELECTRON DEVICES
ATTN SECTRY, WORKING GROUP D
201 VARICK STREET
NEW YORK, NY 10013

AEROSPACE CORPORATION
ATTN M. BIRNBAUM
ATTN N. C. CHANG
ATTN T. S. ROSE
PO BOX 92957
LOS ANGELES, CA 90009

ALLIED ADVANCED APPLICATION DEPT
ATTN A. BUDGOR
31717 LA TIEMDA DRIVE
WESTLAKE VILLAGE, CA 91362

ALLIED SIGNAL INC.
ATTN Y. BAND
ATTN R. MORRIS
POB 1021R
MORRISTOWN, NJ 07960

AMES LABORATORY DOE
IOWA STATE UNIVERSITY
ATTN K. A. GSCHNEIDNER, JR. (2 COPIES)
AMES, IA 50011

ARGONNE NATIONAL LABORATORY
ATTN W. T. CARNALL
9700 SOUTH CASS AVENUE
ARGONNE, IL 60439

BOOZ, ALLEN AND HAMILTON
ATTN W. DROZDOSKI
4330 EAST WEST HWY
BETHESDA, MD 20814

BRIMROSE CORP OF AMERICA
ATTN R. G. ROSEMEIER
7527 BELAIR ROAD
BALTIMORE, MD 21236

DRAPER LAB
ATTN F. HAKIMI
MS 53
555 TECH. SQ
CAMBRIDGE, MA 02139

ENGINEERING SOCIETIES LIBRARY
ATTN ACQUISITIONS DEPT
345 EAST 47TH STREET
NEW YORK, NY 10017

FIBERTECH INC.
ATTN H. R. VERDIN (3 COPIES)
510-A HERNDON PKWY
HERNDON, VA 22070

HUGHES AIRCRAFT COMPANY
ATTN D. SUMIDA
3011 MALIBU CANYON RD
MALIBU, CA 90265

IBM RESEARCH DIVISION
ALMADEN RESEARCH CENTER
ATTN R. M. MACFARLANE (10 COPIES)
MAIL STOP K32 802(D)
650 HARRY ROAD
SAN JOSE, CA 95120

DISTRIBUTION (cont'd)

DIRECTOR
LAWRENCE RADIATION LABORATORY
ATTN M. J. WEBER
ATTN H. A. KOEHLER
ATTN W. KRUPKE
LIVERMORE, CA 94550

MARTIN MARIETTA
ATTN F. CROWNE
ATTN J. LITTLE
ATTN T. WORCHESKY
ATTN D. WORTMAN
1450 SOUTH ROLLING ROAD
BALTIMORE, MD 21227

MIT LINCOLN LAB
ATTN B. AULL
PO BOX 73
LEXINGTON, MA 02173

DEPARTMENT OF MECHANICAL, INDUSTRIAL, &
AEROSPACE ENGINEERING
ATTN S. TEMKIN
PO BOX 909
PISCATAWAY, NJ 08854

NATIONAL OCEANIC & ATMOSPHERIC ADM
ENVIRONMENTAL RESEARCH LABS
ATTN LIBRARY, R-51, TECH RPTS
BOULDER, CO 80302

OAK RIDGE NATIONAL LABORATORY
ATTN R. G. HAIRE
OAK RIDGE, TN 37830

W. J. SCHAFER ASSOC.
ATTN J. W. COLLINS
321 BILLERICA ROAD
CHELMSFORD, MA 01824

SCIENCE APPLICATIONS, INTERNATIONAL CORP
ATTN T. ALLIK
1710 GOODRIDGE DRIVE
McLEAN, VA 22102

UNION CARBIDE CORP
ATTN M. R. KOKTA
ATTN J. H. W. LIAW
750 SOUTH 32ND STREET
WASHOUGAL, WA 98671

ARIZONA STATE UNIVERSITY
DEPT OF CHEMISTRY
ATTN L. EYRING
TEMPE, AZ 85281

CARNEGIE MELLON UNIVERSITY
SCHENLEY PARK
ATTN PHYSICS & EE, J. O. ARTMAN
PITTSBURGH, PA 15213

COLORADO STATE UNIVERSITY
PHYSICS DEPARTMENT
ATTN S. KERN
FORT COLLINS, CO 80523

UNIVERSITY OF CONNECTICUT
DEPARTMENT OF PHYSICS
ATTN R. H. BARTRAM
STORRS, CT 06269

UNIVERSITY OF SOUTH FLORIDA
PHYSICS DEPT
ATTN R. CHANG
ATTN SENGUPTA
TAMPA, FL 33620

JOHNS HOPKINS UNIVERSITY
DEPT OF PHYSICS
ATTN R. R. JUDD
BALTIMORE, MD 21218

KALAMAZOO COLLEGE
DEPT OF PHYSICS
ATTN K. RAJNAK
KALAMAZOO, MI 49007

MASSACHUSETTS INSTITUTE OF TECHNOLOGY
CRYSTAL PHYSICS LABORATORY
ATTN H. P. JENSSEN
ATTN A. LINZ
CAMBRIDGE, MA 02139

MASSACHUSETTS INSTITUTE OF TECHNOLOGY
ATTN V. BAGNATO
ROOM 26-251
77 MASS AVE
CAMBRIDGE, MA 02139

UNIVERSITY OF MINNESOTA, DULUTH
DEPARTMENT OF CHEMISTRY
ATTN L. C. THOMPSON
DULUTH, MN 55813

OKLAHOMA STATE UNIVERSITY
DEPT OF PHYSICS
ATTN R. C. POWELL
STILLWATER, OK 74078

PENNSYLVANIA STATE UNIVERSITY
MATERIALS RESEARCH LABORATORY
ATTN W. B. WHITE
UNIVERSITY PARK, PA 16802

PRINCETON UNIVERSITY
DEPARTMENT OF CHEMISTRY
ATTN D. S. McCLURE
PRINCETON, NJ 08544

DISTRIBUTION (cont'd)

SAN JOSE STATE UNIVERSITY
DEPARTMENT OF PHYSICS
ATTN J. B. GRUBER (20 COPIES)
SAN JOSE, CA 95192

SETON HALL UNIVERSITY
CHEMISTRY DEPARTMENT
ATTN H. BRITTAIN
SOUTH ORANGE, NJ 07099

UNIVERSITY OF VIRGINIA
DEPT OF CHEMISTRY
ATTN DR. F. S. RICHARDSON (2 COPIES)
ATTN DR. M. REID
CHARLOTTESVILLE, VA 22901

UNIVERSITY OF WISCONSIN
CHEMISTRY DEPARTMENT
ATTN J. WRIGHT
ATTN B. TISSUE
MADISON, WI 53706

US ARMY LABORATORY COMMAND
ATTN TECHNICAL DIRECTOR, AMSLC-CT

INSTALLATION SUPPORT ACTIVITY
ATTN LEGAL OFFICE, SLCIS-CC
ATTN S. ELBAUM, SLCIS-CC

USAISC
ATTN TECHNICAL REPORTS
BRANCH, AMSLC-IM-TR (2 COPIES)

HARRY DIAMOND LABORATORIES
ATTN D/DIVISION DIRECTORS
ATTN LIBRARY, SLCHD-TL (3 COPIES)
ATTN LIBRARY, SLCHD-TL (WOODBRIDGE)
ATTN CHIEF, SLCHD-NW-E
ATTN CHIEF, SLCHD-NW-EP
ATTN CHIEF, SLCHD-NW-EH

HARRY DIAMOND LABORATORIES
(cont'd)
ATTN CHIEF, SLCHD-NW-ES
ATTN CHIEF, SLCHD-NW-R
ATTN CHIEF, SLCHD-NW-TN
ATTN CHIEF, SLCHD-NW-RP
ATTN CHIEF, SLCHD-NW-CS
ATTN CHIEF, SLCHD-NW-TS
ATTN CHIEF, SLCHD-NW-RS
ATTN CHIEF, SLCHD-NW-P
ATTN CHIEF, SLCHD-PO
ATTN CHIEF, SLCHD-ST-C
ATTN CHIEF, SLCHD-ST-RS
ATTN CHIEF, SLCHD-TT
ATTN KENYON, C. S., SLCHD-NW-EP
ATTN MILETTA, J. R., SLCHD-NW-EP
ATTN McLEAN, F. B., SLCHD-NW-RP
ATTN LIBELO, L., SLCHD-NW-RS
ATTN BENCIVENGA, A. A., SLCHD-ST-SP
ATTN SATTLER, J., SLCHD-CS
ATTN NEMARICH, J., SLCHD-ST-SP
ATTN WEBER, B., SLCHD-ST-CB
ATTN BAHDER, T., SLCHD-ST-AP
ATTN BENCIVENGA, B., SLCHD-TA-AS
ATTN BRUNO J., SLCHD-ST-AP
ATTN DROPKIN. H., SLCHD-ST-AP
ATTN EDWARDS A., SLCHD-ST-AP
ATTN HAY G., SLCHD-ST-AP
ATTN LEAVITT, R., SLCHD-ST-AP
ATTN PHAM, J., SLCHD-ST-AP
ATTN SIMONIS, G., SLCHD-ST-AP
ATTN STEAD, M., SLCHD-ST-AP
ATTN STELLATO, J., SLCHD-ST-AP
ATTN TOBIN, M., SLCHD-ST-AP
ATTN TOPER, R., SLCHD-ST-AP
ATTN TURNER, G., SLCHD-ST-AP (10 COPIES)
ATTN WORTMAN, D., SLCHD-ST-AP
ATTN GARVIN, C., SLCHD-ST-SS
ATTN GOFF, J., SLCHD-ST-SS
ATTN MORRISON C., SLCHD-ST-AP (10 COPIES)